S1. Detailed information on MRI data acquisition.

All structural MRI scans were performed on the same 3.0-T Magnetom Skyra scanner (Siemens Healthineers, Erlangen, Germany), which is equipped with a standard head coil for radio frequency transmission and reception of nuclear magnetic resonance signal. Participants used soft earplugs and were instructed to relax and remain still. The structural MRI images were acquired with a three-dimensional T1-weighted magnetization-prepared rapid acquisition gradient echo sequence, and scanner parameters were repetition time = 1900ms, echo time = 2.01ms, inversion time = 900ms, flip angle = 9 °, slices=176, matrix size =256×256, contiguous slices with slice thickness =1.0mm, field of view = 256×256mm^2.

S2. Processing procedures of structural MRI image.

The structural images were processed using FreeSurfer 6.0.0 (https://surfer.nmr.mgh.harvard.edu/) with a standard auto-reconstruction procedure, including Talairach registration, intensity normalization, skull-stripping, gray/white matter segmentation, topological deficit correction, and surface deformation[1, 2]. After triangular cortical mesh surfaces representing the white matter surface and pial surface were generated, the reconstructed cortical surfaces were then inspected visually and any inaccuracy in registration or segmentation was corrected according to the instructions (https://surfer.nmr.mgh.harvard.edu/fswiki/FsTutorial/TroubleshootingData) and the cortical reconstruction procedures were repeated until the accurate white matter and pial surface delineation were obtained. Three morphology indexes were calculated here: 1) cortical thickness, quantified as the shortest distance between the white matter surface and pial surface; 2) surface area at each vertex, defined as the averaged area of its surrounding triangles; 3) the cortical folding, defined as the local gyrification index (LGI) measured using Schaer's method [3, 4]. The three morphometric indexes at each ROI were extracted using Freeesurfer's 'aparcstats2table' routine applied to both Desikan-Killiany and Destrieux Atlas, respectively.

S3. Topological properties of the morphometric covariance network.

Studies have shown that brain networks have high efficiency in information transfer, enabling us to adapt to a complicated and changeable environment[5]. In such communication networks, measures such as global efficiency and local efficiency are of importance. Global efficiency is a measure quantifying the whole brain as a singular entity; in morphometric networks, high global efficiency indicates a greater degree of integration in structural covariance. Local efficiency is computed as the inverse of average shortest path length among the neighbours of a node. Local efficiency, in a functional sense, may indicate the speed with which information can be transmitted among neighboring nodes, thus it offers a measure of specialization or segregation. In morphometric networks, high local efficiency indicates a great degree of clustering or segregation (i.e. how much neighbours of a given node are interconnected) of regional structure, indicating a degree of robustness or fault tolerance (whether the neighbours can build a complete graph in the absence of a given node). In the presence of high local efficiency, removal of a sequestered node (or few nodes) would not affect the system in its entirety[6].

The resilience of the morphometric covariance network was evaluated by using random and targeted attacks. Random attack refers to delete one random regional node (and its edges) from the graph and calculating the size of the largest connected component of the network. Targeted attacks refer to remove nodes according to the relative degree of nodes, that is, the first attack is on the most central hub in the network and carried out in descending order of degree.

S4. Detailed information on statistical analysis.

Group-related differences in demographic information were analyzed using SPSS version 26.0 with a significance criterion of $p<0.05$ (2-tailed). Age, education differences were analyzed using two-sample t-tests and sex differences was analyzed using Chi-square test.

The differences of topological properties between groups were examined by non-parametric permutation tests with 1000 repetitions[7, 8]. For each permutation in each group, we randomly reassigned the corrected morphometric index of each subject to one of the two new randomized groups with the same number of subjects as were in the original group and obtained an association matrix for each randomized group. Topological properties at each density were calculated on the whole binary adjacency matrices, which were acquired by thresholding the association matrices at a range of network densities (i.e., 0.3:0.02:0.5). We calculated topological properties at each density of each randomized group to do permutation tests. Functional data analysis (FDA) was adopted to examine group related differences in these curves. In the FDA, each topological property curve is treated as a function ($y = f(x)$), and the sum of differences between groups in y-values was calculated across densities. Then, the statistical *p* values of the actual differences in the curve functions were calculated based on its percentile position. Furthermore, as regional topological properties that were compared across 148 nodes, p-value < 1/148 (i.e., 0.0067) was considered significant in line with prior studies [9, 10]. We used the Brain Connectivity Toolbox to quantify network measures[11] and the Brain NetViewer for network visualization[12].

S5. Relationship between morphometric covariance and childhood trauma.

To explore the influence of childhood trauma, an environmental factor affecting cortical morphology, we first performed correlation analyses relating childhood trauma questionnaire (CTQ) score to the 3 cortical indices in both MDD group and HC group. We then assessed the effect of childhood trauma on the covariance networks as follows: the subjects in MDD group were arranged in order according to CTQ score, and the top 20 MDD patients with higher CTQ score were selected and defined as CTQ-high group, and the last 20 MDD patients with lower CTQ score were defined as CTQ-low group. After extracting the morphological indices for every ROI in the Destrieux Atlas, a linear regression analysis was conducted at every ROI controlling for the effects of age, sex, education, TIV (total intracranial volume), HAMD-17 score, and duration of illness. And then the thickness-based structural covariance networks for these two groups were constructed using the same steps as above. Group comparisons were performed following the procedures described before.

S6. Relationship between morphometric covariance and symptom severity.

We first performed correlation analyses relating symptom severity (HAMD) score to the 3 cortical indices in MDD group. We then assessed the effect of symptom severity on the covariance networks as follows: the subjects in MDD group were arranged in order according to HAMD score, and the top 20 MDD patients with higher HAMD score were selected and defined as HAMD-high group, and the last 20 MDD patients with lower HAMD score were defined as HAMD-low group. After extracting the morphological indices for every ROI in the Destrieux Atlas, a linear regression analysis was conducted at every ROI controlling for the effects of age, sex, education, TIV (total intracranial volume), and duration of illness. Then, the thickness-based structural covariance networks for these two groups were constructed using the same steps as above. Group comparisons were performed following the procedures described before for patients vs. controls analysis.

Appendix 1 to Chen C, Liu Z, Xi C, et al. Multimetric structural covariance in first-episode major depressive disorder: a graph theoretical analysis. *J Psychiatry Neurosci* 2022. doi: 10.1503/jpn.210204

S7. Comparison of female and male participants.

In addition to controlling for sex as a covariate, we also conducted a disaggregated analysis of the global topological properties of the thickness-based graphs in the female and male participants within each group (patients and HCs) and estimated the sex-by-diagnosis interaction.

Patients with MDD: There were no group-related differences between the first-episode female and male patients in global efficiency (female patients=0.681, random-null: mean (SD)=0.683(0.009); male patients=0.686, random-null: mean (SD)=0.683(0.009); p=0.57) and local efficiency (female patients=0.801, random-null: mean (SD)=0.801(0.008); male patients=0.813, random-null: mean (SD)=0.803(0.0078); p=0.23).

Healthy participants: There were no group-related differences between the female HCs and male HCs in global efficiency (female HCs=0.689, random-null: mean (SD)=0.683(0.009); male HCs=0.693, random-null: mean (SD)=0.691(0.003); p=0.25) and local efficiency (female HCs=0.8, random-null: mean (SD)=0.79(0.01); male HCs=0.79, random-null: mean (SD)=0.79(0.01); p=0.52).

Interaction: There were no significant gender-by-diagnosis interactions in global efficiency (p=0.914) and local efficiency (p=0.982).

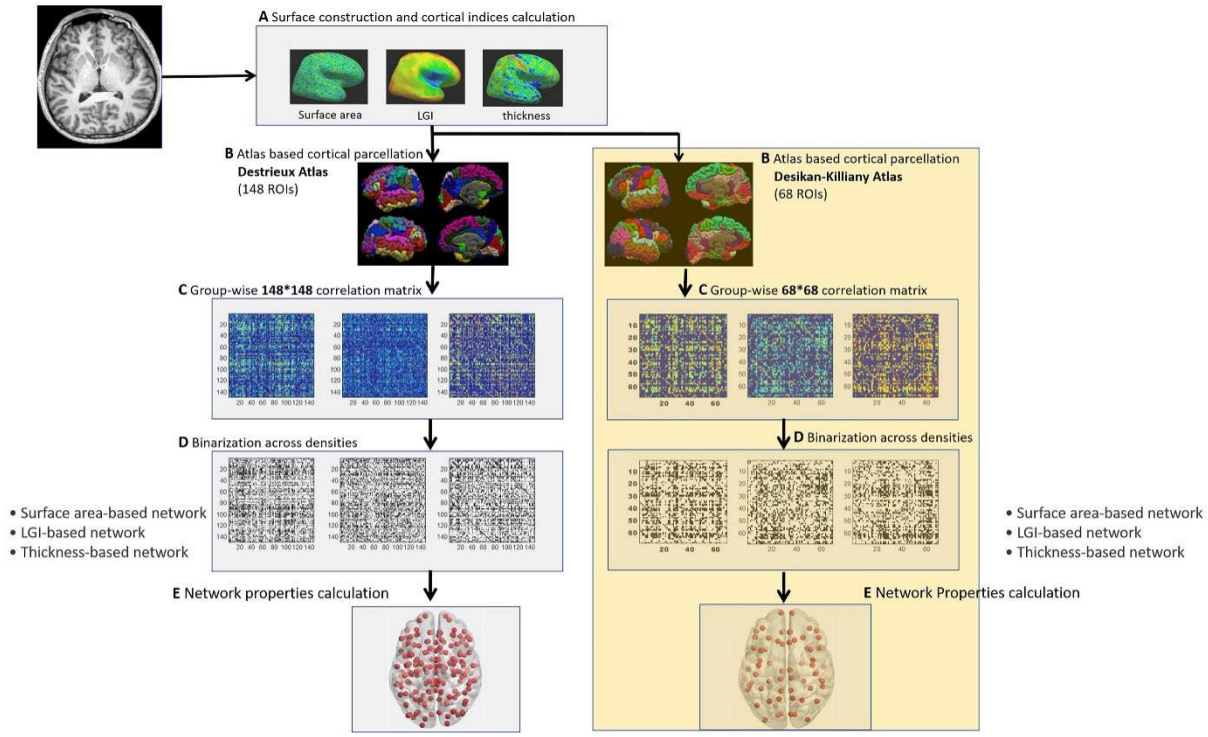

Figure S1. The process of calculating morphometric covariance network properties. LGI: local gyrification index.

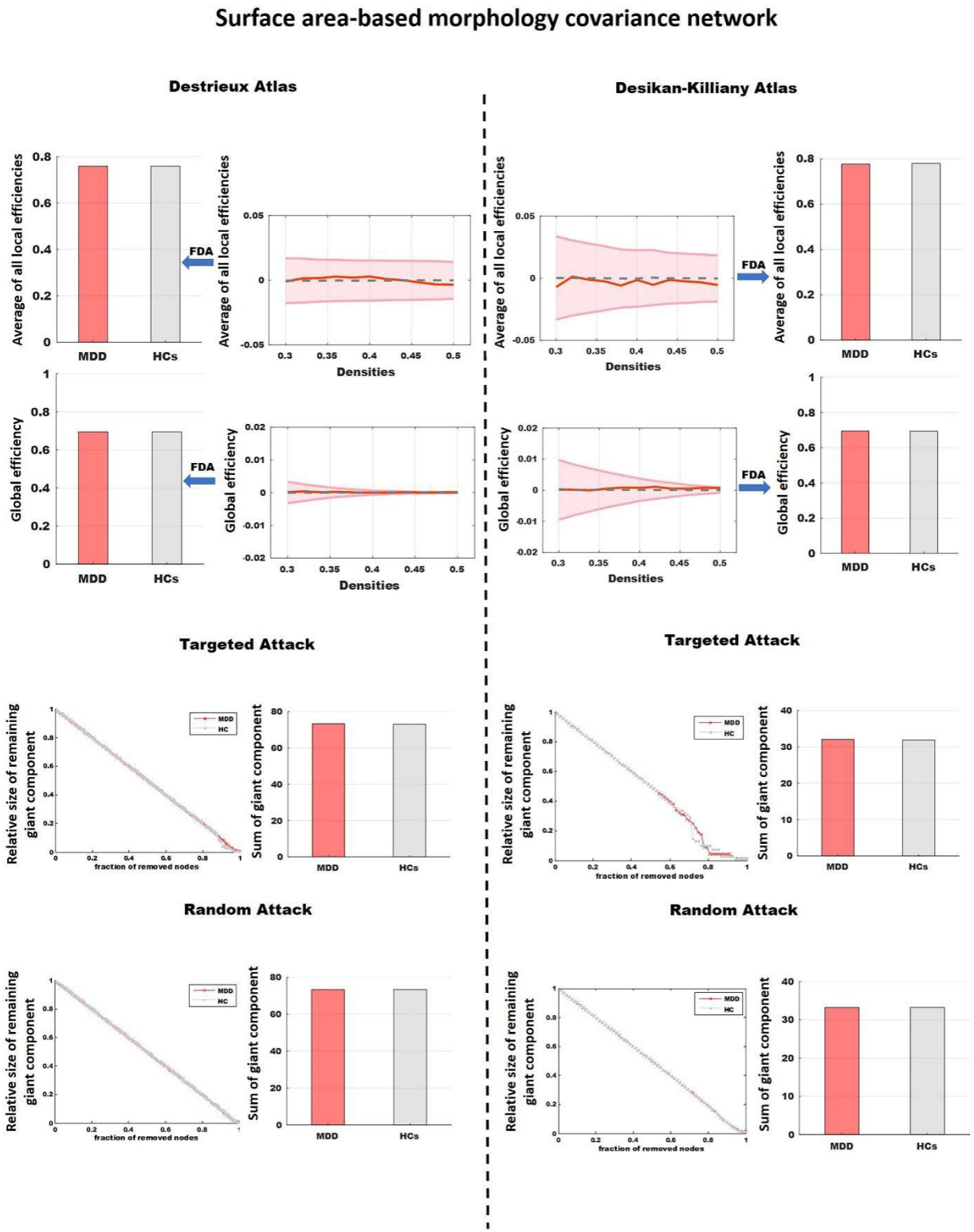

Figure S2. Global properties and Simulated lesion analysis of the surface area-based morphometric covariance network. The **left** panel shows the results of the morphology covariance network constructed on the Destrieux atlas with 148 ROIs, while the **right** panel shows the results of morphology covariance network constructed on Desikan-Killiany Atlas with 68 ROIs, **1)** the upper 2 rows of both right and left panel shows the comparison of topological properties between first-episode MDD group and HC group, with first row shows the comparison of average of all local efficiencies, and the second row shows the comparison of the global efficiency, and no significant difference was detected in surface area-based morphology covariance network; **2)** the bottom 2 rows of both panel shows the results of simulated lesion analysis, including targeted attacks and random attacks, also no significant difference were detected.

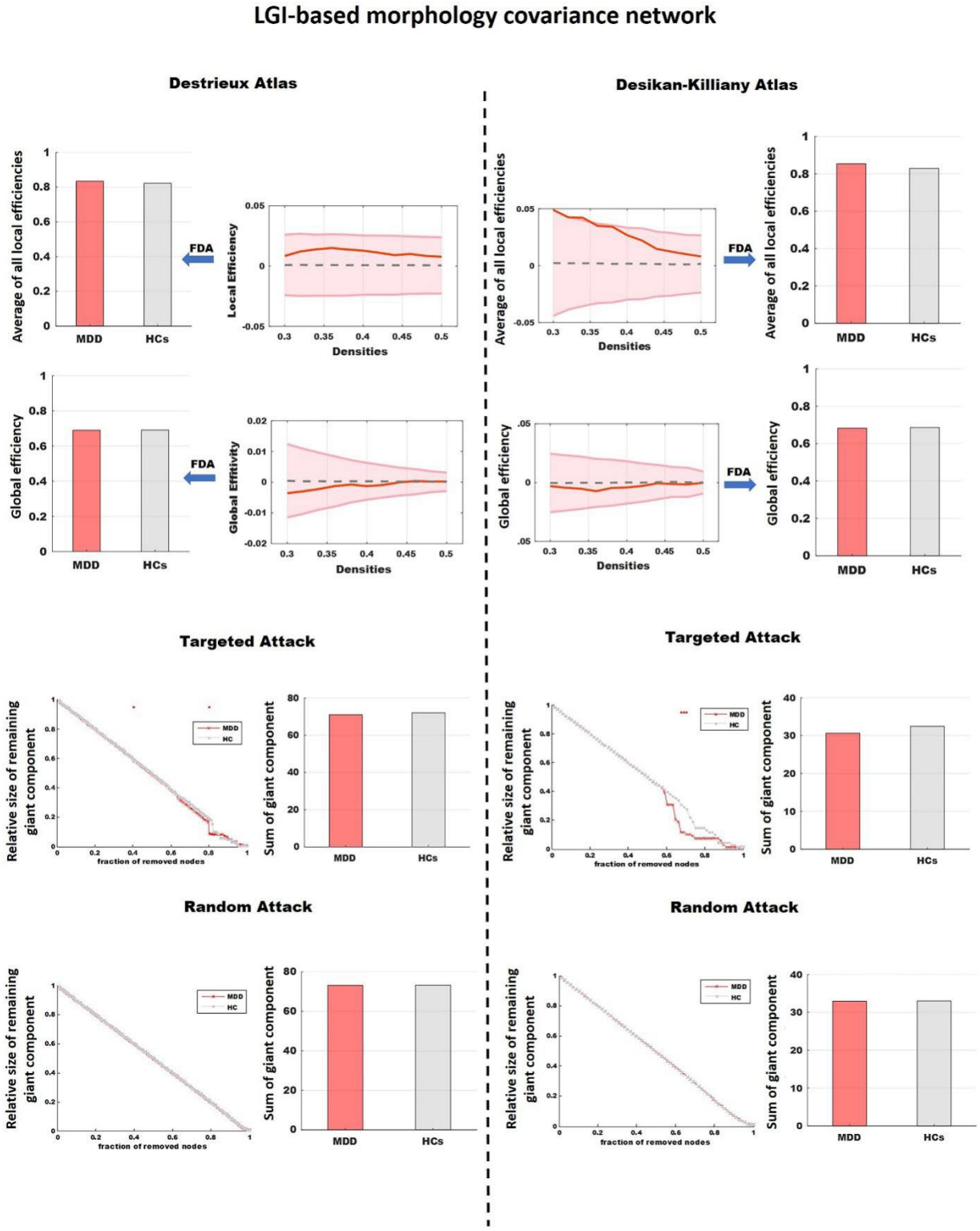

Figure S3. Global properties of the LGI-based morphometric covariance network. The **left** panel shows the results of the morphology covariance network constructed on the Destrieux atlas

with 148 ROIs, while the **right** panel shows the results of morphology covariance network constructed on Desikan-Killiany Atlas with 68 ROIs, **1)** the upper 2 rows of both right and left panel shows the comparison of topological properties between first-episode MDD group and HC group, with first row shows the comparison of average of all local efficiencies, and the second row shows the comparison of the global efficiency, and no significant difference was detected in LGI-based morphology covariance network; **2)** the bottom 2 rows of both panel shows the results of simulated lesion analysis, including targeted attacks and random attacks, also no significant difference were detected. **LGI**: local gyrification index.

Appendix 1 to Chen C, Liu Z, Xi C, et al. Multimetric structural covariance in first-episode major depressive disorder: a graph theoretical analysis. *J Psychiatry Neurosci* 2022. doi: 10.1503/jpn.210204

Table S1. Medication status of the first-episode patients with MDD.

	MDD(n=76)
Medication status	
Drug naïve	49(20/29)
< 7 days medicated	14(7/7)
< 1 month medicated	11(5/6)
< 3 months medicated	1(1/0)
< 6 months medicated	1(0/1)

Note: all data are presented as n(male/female)

Table S2. Global network properties based on morphometric covariance networks constructed from Desikan-Killiany atlas.

Measures	First-episode Patients with MDD (n=76)	HCs (n=66)	*P-value*
	Thickness_based Network		
Local Efficiency			
original	0.783	0.808	0.27
random-null	0.799(0.0177)	0.797(0.018)	
Global Efficiency			
original	0.623	0.684	0.004*
random-null	0.67(0.012)	0.668(0.0134)	
Targeted Attack			
original	25.64	30.56	0.041*
random-null	28.88(1.61)	28.92(1.63)	
Random Attack			
original	32.42	32.55	0.87
random-null	32.04(0.47)	32.07(0.52)	
	Surface_area_based Network		
Local Efficiency			
original	0.78	0.78	0.81
random-null	0.77(0.008)	0.77(0.008)	
Global Efficiency			
original	0.69	0.69	0.678
random-null	0.69(0.0012)	0.694(0.0013)	
Targeted Attack			
original	32.01	31.85	0.764
random-null	32.25(0.54)	32.3(0.54)	
Random Attack			
original	33.23	33.22	0.91
random-null	33.23(0.05)	33.23(0.05)	
	Gyrification_based Network		
Local Efficiency			
original	0.85	0.83	0.172
random-null	0.828(0.0095)	0.826(0.01)	
Global Efficiency			

original	0.683	0.686	0.948
random-null	0.684(0.005)	0.684(0.005)	
Targeted Attack			
original	30.63	32.46	0.19
random-null	31.2(0.98)	31.2(1.04)	
Random Attack			
original	32.92	33	0.78
random-null	32.93(0.17)	32.94(0.17)	

† Note: The global properties (averaged local efficiency and global efficiency) and the resilience (targeted attack and random attack) of the three morphometric covariance networks (thickness-based network, surface area-based network and gyrification-based network) are presented. The data are presented as mean(SD). *represents $p < 0.05$.

Table S3. Nodes with significantly altered local efficiency based on morphometric covariance networks constructed from Desikan-Killiany Atlas (N=68).

Nodes	First-episode Patients with MDD (n=76)	HCs (n=66)	*P-value*
Thickness_based Network			
lh_middle temporal gyrus			
original	0.9	0.78	0.001*
random-null	1.08(0.043)	1.08(0.046)	
lh_Precuneus cortex			
original	0.91	0.83	0.013*
random-null	1.09(0.046)	1.09(0.047)	
lh_Superior frontal gyrus#			
original	0.89	0.77	0.005*
random-null	1.05(0.049)	1.05(0.053)	
lh_Superior temporal gyrus			
original	0.88	0.77	0.008*
random-null	1.04(0.045)	1.04(0.048)	
rh_Paracentral lobule#			
original	0.95	0.83	0.006*
random-null	1.13(0.047)	1.13(0.052)	
rh_Postcentral gyrus			
original	0.97	0.83	0014*
random-null	1.11(0.064)	1.1(0.068)	
rh_Superior frontal gyrus			
original	0.87(0.049)	0.84	0.004*
random-null	1.04	1.04(0.051)	
Surface_area_based Network			
N/A			
Gyrification_based Network			
rh_Caudal middle frontal gyrus			
original	0.6	0.83	0.007*
random-null	1.01 (0.046)	1.01(0.045)	

† Note: the name convention here is comply to the Desikan-Kiliany atlas; * represents p <1/68. # represents the node consistently shown significant difference in local efficiency in both Desikan-Kiliany and Desterieux atlas. The data are presented as mean(SD).

Table S4. The Pearson correlation coefficient of correlation analysis between mean value of cortical indices and Childhood Trauma Questionnaire (CTQ) Score.

	CT	SA	LGI	Comparisons
MDD	0.091(0.069)	0.105(0.073)	0.087(0.063)	SA>LGI; p=0.02; t=-2.3
HC	0.12(0.08)	0.094(0.072)	0.08(0.062)	CT>LGI; p<0.001; t=4.63 CT>SA; p=0.0035; t=2.94
$\Delta R_{HC\ vs.MDD}$	0.029 (t =3.34, p=0.001)	0.011 (t=1.3, p=0.19)	0.007 (t=0.96, p=0.34)	N/A

† Note: The R values presented in the table are the mean obtained by averaging the absolute R values between CTQ scores and individual ROIs (Region of Interest). Data are presented as mean R value (SD), CT: cortical thickness, SA: surface area, LGI: local gyrification index, $\Delta R_{HC\ vs.MDD}$ indicates the change of R value between first-episode patients with MDD and HCs, with t-tests and p-values based on the distribution of correlation coefficients across 148 ROIS in Destrieux atlas.

Table S5. The comparison of the global efficiency of thickness covariance networks constructed from Destrieux atlas between patients with high CTQ and patients with low CTQ.

Global Efficiency	**First-episode MDD Patients with High CTQ (N=20)**	**First-episode MDD Patients with Low CTQ (N=20)**	***P-value***
original	0.503	0.56	0.042
random-null	0.543(0.02)	0.541(0.021)	

Table S6. The Pearson correlation coefficient of correlation analysis between mean value of cortical indices and HAMD total score.

CT	SA	LGI	Comparisons
0.101(0.08)	0.103(0.071)	0.109(0.081)	p=0.64; F=0.45

† Note: The R values presented in the table are the mean obtained by averaging the absolute R values between HAMD scores and individual ROIs (Region of Interest), with t-tests and p-values based on the distribution of correlation coefficients across 148 ROIS in Destrieux atlas. Data are presented as mean R value (SD), CT: cortical thickness, SA: surface area, LGI: local gyrification index.

Appendix 1 to Chen C, Liu Z, Xi C, et al. Multimetric structural covariance in first-episode major depressive disorder: a graph theoretical analysis. *J Psychiatry Neurosci* 2022. doi: 10.1503/jpn.210204

Table S7. The comparison of the network properties of thickness covariance networks constructed from Destrieux atlas between patients with high HAMD and patients with low HAMD scores.

Measures	First-episode MDD Patients with High HAMD (N=20)	First-episode MDD Patients with Low HAMD (N=20)	*P-value*
Global Efficiency			
original	0.66	0.677	0.393
random-null	0.668(0.008)	0.667(0.011)	
Local Efficiency			
original	0.79	0.801	0.367
random-null	0.797(0.008)	0.797(0.008)	

References

1. Dale, A.M., B. Fischl, and M.I. Sereno, *Cortical surface-based analysis. I. Segmentation and surface reconstruction.* Neuroimage, 1999. **9**(2): p. 179-94.
2. Fischl, B., M.I. Sereno, and A.M. Dale, *Cortical surface-based analysis. II: Inflation, flattening, and a surface-based coordinate system.* Neuroimage, 1999. **9**(2): p. 195-207.
3. Schaer, M., et al., *How to measure cortical folding from MR images: a step-by-step tutorial to compute local gyrification index.* J Vis Exp, 2012(59): p. e3417.
4. Schaer, M., et al., *A surface-based approach to quantify local cortical gyrification.* IEEE Trans Med Imaging, 2008. **27**(2): p. 161-70.
5. Bullmore, E.T. and O. Sporns, *Complex brain networks: graph theoretical analysis of structural and functional systems.* Nature Reviews Neuroscience, 2009. **10**(3): p. 186-198.
6. Achard, S. and E.T. Bullmore, *Efficiency and cost of economical brain functional networks.* Plos Computational Biology, 2007. **3**(2): p. 174-183.
7. He, Y., Z. Chen, and A. Evans, *Structural insights into aberrant topological patterns of large-scale cortical networks in Alzheimer's Disease.* Journal of Neuroscience, 2008. **28**(18): p. 4756-4766.
8. Bassett, D.S., et al., *Hierarchical organization of human cortical networks in health and schizophrenia.* Journal of Neuroscience, 2008. **28**(37): p. 9239-9248.
9. Lynall, M.E., et al., *Functional connectivity and brain networks in schizophrenia.* J Neurosci, 2010. **30**(28): p. 9477-87.
10. Yang, J., et al., *Connectomic signatures of working memory deficits in depression, mania, and euthymic states of bipolar disorder.* J Affect Disord, 2020. **274**: p. 190-198.
11. Rubinov, M. and O. Sporns, *Complex network measures of brain connectivity: Uses and interpretations.* Neuroimage, 2010. **52**(3): p. 1059-1069.
12. Xia, M.R., J.H. Wang, and Y. He, *BrainNet Viewer: A Network Visualization Tool for Human Brain Connectomics.* Plos One, 2013. **8**(7).